IEEE Access
Multidisciplinary | Rapid Review | Open Access Journal

Received August 5, 2018, accepted September 16, 2018, date of publication November 9, 2018,
date of current version December 7, 2018.

Digital Object Identifier 10.1109/ACCESS.2018.2876641

Practical Residual Interference After Cancellation for Constant Envelope Modulation With Data-Aided Synchronization

QIONGJIE LIN[1] AND MARY ANN WEITNAUER[2], (Senior Member, IEEE)
[1]Samsung Research America Inc., Mountain View, CA 94043, USA
[2]School of Electrical and Computer Engineering, Georgia Tech, Atlanta, GA 30332, USA

Corresponding author: Qiongjie Lin (qiongjie.l@samsung.com)

This work was supported in part by the Georgia Research Alliance of the State of Georgia and in part by the U.S. National Science Foundation under Grant CNS-1513884.

ABSTRACT Interference cancellation (IC) is a well-known technique for improving bandwidth utilization in wireless networks. In this paper, we evaluate the practical residual interference of IC with constant envelope modulation in a flat fading environment for a low-power wide area wireless sensor network application, both analytically and experimentally. We propose a new model for the residual interference power, which is the power of the packet being canceled times a random variable. We derive the mean, variance, and distribution of the random variable considering the arbitrary overlapping scenario between two packets with one-time IC. Then, we show how the method can be applied recursively to model the residual interference power when multiple packets are canceled in ordered successive IC. In contrast to the conventional model, we find that this factor varies for different overlapping scenarios and is a function of the signal-to-interference-and-noise ratio of the preamble of the packet being canceled and of the overlapping degree. The theoretical statistics of the residual interference assume maximum likelihood estimation of synchronization offsets.

INDEX TERMS Interference cancellation, software-defined radio, synchronization error, wireless sensor network.

I. INTRODUCTION

Interference cancellation (IC) dates back to the 1990's [1]–[3]. IC is attractive because it allows multiple co-channel packets occurring at the same time to be decoded by a single-antenna receiver, resulting in significantly improved reliability and throughput. In IC, the effects of a decoded strong packet are subtracted from stored samples of the received signal, thereby making possible the capture of weaker packets. However, because of imperfect synchronization and channel estimation, the subtraction leaves a residual interference, which causes interference on the weaker packets. In the networking literature, some recent works ignore this interference [4], [5] or they model its power very simply as a fixed percentage of the power of the packet being canceled [6], [7]. We refer to the latter case as the "conventional model". However, through theory and experiment, we find that other parameters are very important, particularly the signal-to-interference-plus-noise ratio (SINR) on the preamble of the packet being canceled. These observations have led us to the main contribution of this paper: a new physical layer statistical model for IC residual interference in packet networks that use constant envelope modulation.

IC has been shown to improve bandwidth utilization in cellular networks [8], which have centralized control and synchronized clocks among wireless devices, and where the towers determine the best transmit power, coding rate and/or spreading codes to enable the disambiguation of different up-link transmissions. However, in the low power wide area wireless sensor networks we are considering, particularly networks with extremely energy-efficient transmit-only sensors [9], [10], there is no centralized control over power, no time and frequency synchronization between wireless devices, and in general the techniques to facilitate the disambiguation at transmitter side are constrained by the physical limitations of wireless sensors. In this work, we are interested in the uplink transmission of wireless sensor networks for low-power, long-range radio applications. The application of IC to the low end market is a breakthrough and is not widely adopted in commercial market yet due to the high complexity of IC processing and limited power consumption

in the sensor network. However, it becomes promising as the overhead of IC can be shifted to the gateway, which can be a software-defined radio with strong computation capability [11]. Meanwhile, an interference-insensitive synchronization scheme has been proposed for reliable packet detection and compensation of large RF impairments [12] for transmit-only wireless sensor networks.

Several recent reports of IC experiments exist [13]–[15], including for Zigbee networks [16]. In [15], successive interference cancellation (SIC) with carrier sense threshold is adapted to work in uncontrolled network scenarios for the IEEE 802.15.4 (ZigBee). However, all these studies focus on the packet delivery rate improvement of SIC in WLANs, by handling the hidden terminals problem. These studies do not focus on characterizing the residual interference. In [12], we report preliminary experiment results on practical residual interference of IC for MSK for just two packets overlapping, and the corresponding theoretical analysis is ignored. This paper treats the more general case of constant envelope modulation, treats an arbitrary number of overlapping packets, and includes theoretical analysis.

Regarding theoretical analysis, the statistics and probability density function of the residual interference of IC was studied in [17] and [18] for CDMA systems and satellite communications. However, they only considered the residual interference caused by imperfect channel estimation but not synchronization error, and also only simulation was performed.

In addition to the requirement of high spectral efficiency, energy efficiency (or equivalently battery duration), is another important requirement of most wireless communication systems. For instance, in the lower power wide area (LPWA) application, energy efficiency is more crucial to achieve high-coverage, low-cost per connection, and years-long battery life [19], [20]; LPWA has evolved to become an essential component of Internet of things (IoT), a popular topic of next generation wireless communications. Constant envelope modulations, such as FSK, GFSK, MSK, GMSK, are widely used in low power RF transceivers [21]–[23] to enhance and improve the energy efficiency of wireless communication networks, as they allow the power amplifiers of transceiver to operate at or close to the saturation level to maximize energy efficiency. On the other hand, the more advanced modulations, such as QAM, contain amplitude modulation (AM) components, which require from 3 to 6 dB of back off (from saturation) in the output power amplifier [24].

In this paper, we study both experimentally and theoretically, the practical residual interference of IC at the gateway for constant envelope modulation by considering the effects of both imperfect synchronization and channel estimation. Assuming overlapping packets are ordered from strongest to weakest. We derive a novel statistical model for the average power of the interference that the residual of the kth previously canceled packet makes on the nth packet to be decoded. The statistics are the mean, variance, and probability density function of the factor, $g_{k,n}$, such that $g_{k,n}P_k$ is the average power of the interference, while P_k is the power of kth canceled packet. We show that the statistics of $g_{k,n}$ vary significantly with the SINR of the kth packets' preamble and with the degree of overlap of packets. We experimentally investigate the characteristics of the residual interference for unsynchronized packets modulated with minimum shift keying (MSK) and that begin with a pseudo-noise preamble, followed by a MSK payload. This signal design is appropriate for some Internet of Things (IoT) applications in unlicensed bands, including severely power constrained transmit-only and beaconing devices [25]–[28]. We show that the characteristics of practical residual interference deviates significantly from the simple conventional model.

The rest of the paper is organized as follows. Section II describes the system model. Section III theoretically analyzes the practical residual interference. The simulation results are compared with the analytical results in Section IV. In Section V, we report experimental results based on software-defined radios. Section VI concludes the paper.

II. SYSTEM MODEL

We study the uplink of the random access wireless network illustrated in Fig.1. The system is composed of many randomly distributed low power transmitters and a single-antenna gateway (GW). We assume that the GW always stores the latest K samples it received, where K is at least large enough to include a packet and the processing time to decode and cancel a packet. With IC, when a packet has been decoded by the GW, the packet's physical layer samples are synthesized or regenerated and subtracted from the stored samples.

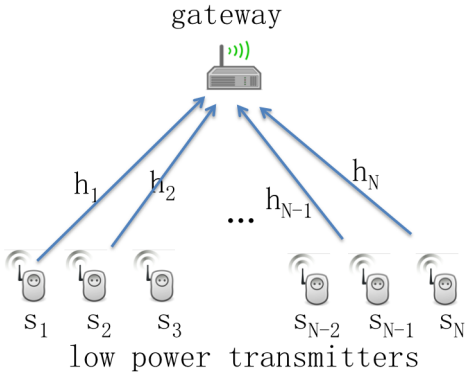

FIGURE 1. Illustration of the network architecture.

As we address low power transmitters for LPWA application, constant envelope modulation (CEM) is assumed for the benefit of high power efficiency. The popular CEMs are FSK, GFSK, MSK and GMSK. In our physical layer model, each packet is composed of only two parts: a known preamble and a payload of random data. The preamble is a binary PN sequence, L_1 bits long, while the payload is

composed of L2 information symbols that are generally M-ary (i.e., carrying more than one bit per symbol). We adopt the synchronization scheme presented in [29].

The complex baseband signal with continous phase modulation (CPM) from a transmitter can be expressed as

$$x(t) = \sqrt{\frac{2E_c}{T_c}} exp\{j\phi(t;\alpha)\}, \tag{1}$$

where E_c is the energy per transmitted symbol with duration T_c. $\phi(t;\alpha)$ is the phase of the signal, which is represented as

$$\phi(t;\alpha) = 2\pi d \sum_{i=0}^{L-1} \alpha_i q(t - iT_c), \tag{2}$$

where α_i is a sequence $\{\alpha_0, \alpha_1, \ldots, \alpha_{L-1}\}$ of bits such that $\alpha_i \in \{\pm 1, \pm 3, \ldots, M-1\}$ [30]. L is the total number of symbols for one packet, so that $L = L_1 + L_2$. The variable d is the modulation index of CPM. The waveform $q(t)$ is the phase response of the modulation.

We assume a flat fading channel, modeled as $h = \gamma e^{j\theta}$, where γ is the magnitude and θ is the phase. The complex baseband representation of the received signal is

$$y(t) = e^{j(2\pi f_d t)} hx(t - \tau) + z(t), \tag{3}$$

where f_d is the frequency offset, τ is the timing offset, and $z(t)$ is complex baseband AWGN with zero mean and power spectral density N_0. In practice, $y(t)$ is sampled N times per symbol with sampling rate of f_s. This results in a discrete-time version of received signal as

$$y[i] = y(\frac{iT_c}{N}) = e^{j(2\pi\omega i)} hx[i] + z[i], \tag{4}$$

where $\omega = f_d T_c / N$ is the normalized frequency offset with respect to the sampling frequency. $x[i] = x(\frac{iT_c}{N} - \tau)$ and $z[i]$ are the sampled versions of $x(t-\tau)$ and $z(t)$, respectively.

We consider the case of $N > 1$ packets overlapping at the receiver with different powers. Because of the independence of data in different packets, the powers of the overlapped packets are superimposed in time domain. For the purpose of description, we index the packets from strongest to weakest as illustrated in Fig.2. In practice, with the data-aided synchronization [29], [31], the start of the packet (SOP) can be identified through frame synchronization based on the received preamble in a packet network. If the value of SOP detection metric at sample index i is larger than a threshold V_0, which is a system design parameter, then we can claim that there exists a packet started at sample index i. In [29], an interference-insensitive synchronization algorithm was proposed to address the LPWA sensor applications with low-power transmit-only sensors. The SOPs for three overlapped packets with equal received SNR are shown to be distinct through simulations [29]. Similar results are observed in our experiments as shown in Fig.9 in Section V.

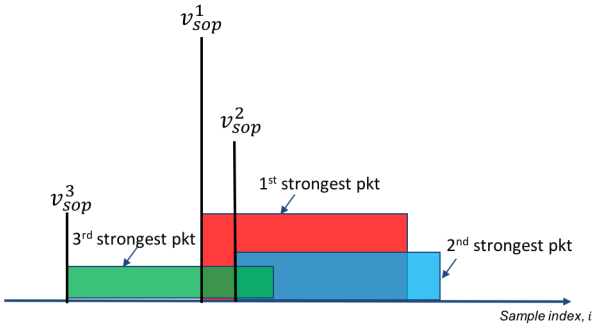

FIGURE 2. Illustration of N packets overlapping (N = 3).

Algorithm 1 Practical SIC

1) Initialize the iteration counter, $n = 1$;
2) Perform synchronization on the received samples, which outputs the SOP detection metric value, v_i^n, for each sample index, i, in current nth iteration;
3) Identify the SOP of nth strongest packet, indicated by the highest value of v_i^n at location I_s^n, s.t, $v_{sop}^n = v_{I_s^n}^n = max\{v_i^n\}$;
4) If $v_{sop}^n > V_0$, declare packet detected; go to Step 5), otherwise exit;
5) Decode nth strongest. If successful, go to step 6), otherwise exit;
6) Regenerate the clean samples of the nth strongest packet and subtract out the clean samples from the received samples, $n = n + 1$, and go to Step 2)

In this context, successive IC (SIC) can be performed to decode the multiple interfered packets iteratively. The concept of SIC is well known. We summarize it here, in terms of our practical SOP detection procedure.

In this way, the IC processing of decoding and subtracting out the present strongest packet can be repeated iteratively until we fail on detecting or decoding the next strongest packet. The SINR of the nth packet processed during the nth iteration is typically modeled as [7]:

$$SINR_n = \frac{P_n}{\sum_{k=1}^{n-1} g_{k,n} P_k + \sum_{k=n+1}^{N} P_k + \sigma_n^2}, \tag{5}$$

where P_n is the averaged received signal power of the nth packet, and $g_{k,n}P_k$ is the residual interference from the kth packet imposed on the nth packet caused by imperfect IC during the kth iteration. The second sum in Eq.(5) is the interference from uncanceled packets that are weaker than the nth packet.

We note that one of the main contributions of this paper is showing how $g_{k,n}$ depends on $SINR_k^p$, which is the SINR of the preamble of the kth packet, and $O_{n,k}$, which is the degree of overlap between the nth and kth packets. These statistics for $g_{k,n}$ are useful to model the physical layer performance in network-level simulations, which typically declare a packet decoded if its $SINR$ is above a specified threshold.

III. PRACTICAL RESIDUAL INTERFERENCE MODEL

In this section, we first evaluate the instantaneous residual interference at the receiver. Because the residual interference is the error of the estimate of the waveform to be canceled, in the sequel, we refer to the residual interference as the residual error. Next, we derive the exact model of the practical residual error factor, $g_{k,n}$, from an intermediate variable, residual-error-to-signal-ratio (ESR). The ESR is defined based on the instantaneous residual error, and is measured through experiments in next section. Finally, we establish an approximate model for the statistics of $g_{k,n}$, which is essential for network performance analysis.

A. INSTANTANEOUS RESIDUAL ERROR

In practical IC, the subtraction of the decoded packet is not perfect due to the imperfect synchronization and channel estimation. An interference-insensitive timing synchronization approach is available [29], therefore we assume the timing synchronization is perfect. Let $\omega, \hat{\omega}$ be the real and estimated normalized carrier frequency offsets (CFOs), respectively, between the TX and GW. Let $\hat{h} = \hat{\gamma}e^{j\hat{\theta}}$ be the estimated channel. The residual IC error at sample index i for the successfully decoded packet $y[i]$ after subtracting the reconstructed signal $\hat{y}[i]$ becomes:

$$\begin{aligned} e[i] &= e^{j(2\pi\omega i)}hx[i] - e^{j(2\pi\hat{\omega}i)}\hat{h}x[i] \\ &= x[i]\left(\gamma e^{j(2\pi\omega i+\theta)} - \hat{\gamma}e^{j(2\pi\hat{\omega}i+\hat{\theta})}\right). \end{aligned} \tag{6}$$

Let $\beta_i = 2\pi\omega i + \theta$, $\hat{\beta}_i = 2\pi\hat{\omega}i + \hat{\theta}$, and $\Delta\beta_i = \beta_i - \hat{\beta}_i$. Then the magnitude squared of the residual error is

$$\begin{aligned} |e[i]|^2 &= e[i]e^*[i] \\ &= |x[i]|^2\left(\gamma^2 + \hat{\gamma}^2 - \gamma\hat{\gamma}e^{j\Delta\beta_i} - \hat{\gamma}\gamma e^{-j\Delta\beta_i}\right) \\ &= |x[i]|^2\left(\gamma^2 + \hat{\gamma}^2 - 2\gamma\hat{\gamma}cos(\Delta\beta_i)\right). \end{aligned} \tag{7}$$

Define the errors in the channel and CFO estimates to be $e_\gamma = \gamma - \hat{\gamma}, e_\theta = \theta - \hat{\theta}, e_\omega = \omega - \hat{\omega}$, respectively. The expectation of instantaneous residual error after cancellation becomes

$$E\{|e[i]|^2\} = \sigma_s^2 E\left\{\gamma^2 + \hat{\gamma}^2 - 2\gamma\hat{\gamma}cos(2\pi e_\omega i + e_\theta)\right\}, \tag{8}$$

where σ_s^2 is the average transmitted signal power. According to Eq.(8), the instantaneous residual error is not constant over the packet, and but a function of time determined by the errors in the estimates of channel gain, frequency and phase. For larger sample index i, the residual error tends to be larger due to the larger accumulated phase offset $\Delta\beta_i = 2\pi e_\omega i + e_\theta$.

B. DERIVATION OF $g_{k,n}$

Recall $g_{k,n}P_k$ is the residual error of the kth previously canceled packet on the present packet to be decoded, packet n. In the following, we will refer to the kth packet as the "strong" packet and the nth packet as the "weak" packet. We consider how g varies with respect to $O_{k,n}$ and $SINR_k^P$ of the kth strong packet preamble.

We define an intermediate variable, the residual-error-to-signal-ratio (ESR), which is the average power of residual error over the overlapping interval, normalized by the average received power of the stronger packet over the same overlapping interval. It may be expressed as

$$ESR_{k,n} = \frac{E\{\sum_{I_s^k}^{I_e^k}|e_k[i]|^2/N_{ov}\}}{E\{\sum_{I_s^k}^{I_e^k}|y_k[i]|^2/N_{ov}\}} = \frac{E\{\sum_{i=I_s^k}^{I_e^k}|e_k[i]|^2\}}{P_k N_{ov}}, \tag{9}$$

where I_s^k is the starting sampling index of the overlapped portion of the kth packet, I_e^k is the ending sampling index of the portion, N_p is the number of packet samples, $N_{ov} = I_e^k - I_s^k$ is the number of overlapping samples, and $O_{k,n} = \frac{N_{ov}}{N_p}$ is the overlapping degree. It follows that

$$g_{k,n} = O_{k,n} * ESR_{k,n}. \tag{10}$$

By substituting the instantaneous residual error from Eq.(8), the ESR can be written as

$$\begin{aligned} ESR_{k,n} = \frac{1}{P_s N_{ov}}\Bigg(&\sigma_k^2\gamma^2 N_{ov} + \sigma_k^2\hat{\gamma}^2 N_{ov} \\ &- 2\sigma_k^2\gamma\hat{\gamma}E\{\sum_{I_s^k}^{I_e^k} cos(2\pi e_\omega i + e_\theta)\}\Bigg), \end{aligned} \tag{11}$$

$$= 1 + \xi - 2\hat{\xi}\frac{E\{\sum_{I_s^k}^{I_e^k} cos(2\pi e_\omega i + e_\theta)\}}{N_{ov}}, \tag{12}$$

where, σ_k^2 is the average transmit power for the kth packet, and $\xi = \frac{\sigma_k^2\hat{\gamma}^2}{P_k}$ and $\hat{\xi} = \frac{\sigma_k^2\gamma\hat{\gamma}}{P_k}$ are ratios of received signal power estimates based on estimated channel gain to the real received signal power.

By applying the Lemma: $\sum_{k=0}^{n} cos(ak + z) = csc(\frac{a}{2})sin(\frac{1}{2}a(n+1))cos(\frac{an}{2} + z)$ [32] into Eq.(12), the ESR then becomes:

$$ESR_{k,n} = 1 + \xi - 2\hat{\xi} * K(e_\omega, e_\theta, O_{k,n}, I_s^k, I_e^k), \tag{13}$$

where

$$\begin{aligned} &K(e_\omega, e_\theta, O_{k,n}, I_s^k, I_e^k) \\ &= \underbrace{\frac{sin(\pi e_\omega O_{k,n}N_p)}{sin(\pi e_\omega)O_{k,n}N_p}}_{C_1} * \underbrace{cos(\pi e_\omega(I_e^k + I_s^k) + \pi e_\omega + e_\theta)}_{C_2} \end{aligned} \tag{14}$$

In reality, there are two types of overlapping scenarios between the nth and kth packets as illustrated in Fig.3: the strong leading (SL) case and the weak leading (WL) case. For the SL case, $I_e^k = N_p$ is fixed, and $I_s^k = I_e^k - O_{k,n}N_p = N_p(1 - O_{k,n})$, while for WL case, $I_s^k = 1$ is fixed, and $I_e^k = I_s^k + O_{k,n}N_p = N_p O_{k,n} + 1$.

Therefore, the sub-term C_2 in Eq. (14) can be derived accordingly for SL and WL cases, and the intermediate key term K with expression of Eq.(14) can be re-written

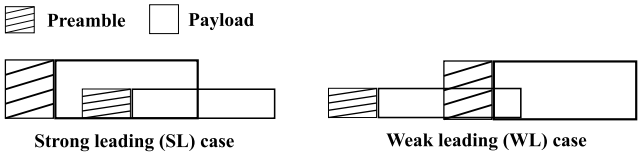

FIGURE 3. Illustration of overlapping scenarios.

for different overlapping cases as

$$K^{SL} = C_1 C_2^{SL}, \tag{15}$$
$$K^{WL} = C_1 C_2^{WL}, \tag{16}$$
$$C_2^{SL} = cos\Big(-\pi e_\omega N_p O_{k,n} + 2\pi e_\omega N_p + \pi e_\omega + e_\theta \Big), \tag{17}$$
$$C_2^{WL} = cos\Big(\pi e_\omega N_p O_{k,n} + 3\pi e_\omega + e_\theta \Big). \tag{18}$$

C. APPROXIMATE ERROR MODEL

In the literature, there are many data-aided synchronization schemes proposed based on unbiased ML estimation algorithms. The Cramer-Rao Bound of the residual error is often studied to evaluate the performance in terms of the length of training sequence and SNR condition. We adopted the closed form of the variance for the normalized frequency and phase synchronization errors [33], [34], which are simplified at high SNR as:

$$\begin{cases} e_\omega = \dfrac{\hat{f}_d - f_d}{f_s} \sim N(0, \sigma_\omega^2), & \sigma_\omega^2 \simeq \dfrac{3}{2\pi^2 L_1^3 N^2 SINR_k^p} \\ e_\theta = \dfrac{\hat{\theta} - \theta}{\pi} \sim N(0, \sigma_\theta^2), & \sigma_\theta^2 \simeq \dfrac{1}{2\pi^2 L_1 SINR_k^p} \end{cases} \tag{19}$$

where L_1 is the number of symbols on the preamble for synchronization, N is the sampling factor (number of samples per symbol), and $SINR_k^p$ is the SINR on the preamble of the kth strong packet.

As the number of packet samples, N_p, is very large, while the normalized frequency synchronization error, e_ω is very small, the last two terms within the cosine function in both Eq.(17) and Eq.(18) are negligible, and C_1 in Eq.(14) can be approximated by the $sinc(x) = \frac{sin(\pi x)}{\pi x}$ function. Therefore the parameter K for the two overlapping cases then becomes,

$$K^{SL} = sinc(O_{k,n}) \underbrace{cos(-O_{k,n} + 2X)}_{C_2^{SL}}, \tag{20}$$
$$K^{WL} = sinc(O_{k,n}) \underbrace{cos(O_{k,n})}_{C_2^{WL}}, \tag{21}$$

where, $X = N_p e_\omega$.

Consider the quadratic approximations of sinc and cosine functions based on the Taylor expansions [35]:

$$cos(X) = \sum_{k=0}^{\infty} \frac{(-1)^k X^{2k}}{(2k+1)!} \simeq 1 - \frac{X^2}{3!} + \mathcal{O}(X^4) \tag{22}$$
$$sinc(X) = \sum_{k=0}^{\infty} \frac{(-1)^k X^{2k}}{(2k)!} \simeq 1 - \frac{X^2}{2} + \mathcal{O}(X^4) \tag{23}$$

Thus, the intermediate term K used in practical residual error models can be approximated as

$$K^{SL} \simeq 1 - \frac{6 + 2O_{k,n}^2 - 6O_{k,n}}{3} X^2 - \frac{4O_{k,n}^2 + O_{k,n}^4 - 4O_{k,n}^3}{12} X^4 \tag{24}$$
$$K^{WL} \simeq 1 - \frac{2O_{k,n}^2}{3} X^2 + \frac{O_{k,n}^4}{12} X^4 \tag{25}$$

Define $Y = X^2$ and assume the channel gain estimates are perfect and that $\xi = \hat{\xi} = 1$. The g is then simplified as

$$g^{SL} = A_1^{SL} Y^2 + A_2^{SL} Y \tag{26}$$
$$g^{WL} = A_1^{WL} Y^2 + A_2^{WL} Y \tag{27}$$

where,

$$\begin{cases} A_1^{SL} = \dfrac{1}{6}(-O_{k,n}^4 + 4O_{k,n}^3 - 4O_{k,n}^2), \\ A_2^{SL} = \dfrac{2}{3}(2O_{k,n}^2 - 6O_{k,n} + 6). \end{cases} \tag{28}$$

$$\begin{cases} A_1^{WL} = \dfrac{-1}{6} O_{k,n}^4, \\ A_2^{WL} = \dfrac{4}{3} O_{k,n}^2. \end{cases} \tag{29}$$

It is straightforward to show that, $Y = X^2 \sim Gamma(\alpha, \beta)$ with α as the shape parameter and β as the rate parameter. The pdf of Y is

$$f_Y(y) = \frac{\beta^\alpha y^{\alpha-1} e^{-\beta y}}{\Gamma(\alpha)},$$
$$\alpha = \frac{1}{2}, \beta = \frac{1}{2\sigma_X^2} = \frac{1}{2N_p^2 \pi^2 \sigma_\omega^2} = \frac{L\epsilon^3 SINR_k^p}{3}, \tag{30}$$

where L is the total number of information bits of the packet, and $L_1 = \epsilon L$ is the number of information bits of the preamble, and $SINR_k^p$ is the SINR of the strong kth packet preamble.

According to the expression of ESR in Eq.(26), and (27), ESR is a function of RV, Y, with a Gamma distribution. We then define the other new RV, $Z = A_1 Y^2 + A_2 Y$; it has the derived pdf, $f_Z(z)$, as

$$f_Z(z; A_1, A_2) = \sum_{i=1}^{2} \frac{f_Y(y_i)}{|\frac{dz}{dy}|_{y=y_i}} = \sqrt{\frac{\beta}{\pi(A_2^2 + 4A_1 z)}} \left(y_1^{-\frac{1}{2}} e^{y_1 \beta} + y_2^{-\frac{1}{2}} e^{-y_2 \beta} \right) \tag{31}$$

with

$$y_1 = \frac{-A_2 + \sqrt{A_2^2 + 4A_1 z}}{2A_1}, \quad y_2 = \frac{-A_2 - \sqrt{A_2^2 + 4A_1 z}}{2A_1}. \tag{32}$$

Therefore, the pdf of $g_{k,n}$ for the two overlapping cases are $f_{g^{SL}} = f_z(z; A_1^{SL}, A_2^{SL}), f_{g^{WL}} = f_z(z; A_1^{WL}, A_2^{WL})$ with corresponding parameters substitutions of A_1, A_2 in Eq. (32).

1) FIRST MOMENT STATISTICS, **MEAN**, μ_Z

Given the mean, $E[Y] = \frac{\alpha}{\beta}$ and variance, $Var[Y] = \frac{\alpha}{\beta^2}$, of the gamma distributed Y, the first moment of the derived RV Z can be computed as

$$\begin{aligned}\mu_Z &= E[Z; A_1, A_2] \\ &= A_1 E[Y^2] + A_2 E[Y] \\ &= A_1(Var[Y] + E[Y]^2) + A_2 E[Y], \\ &= \frac{A_1}{\beta^2}(\alpha^2 + \alpha) + \frac{A_2\alpha}{\beta} = \frac{3A_1}{4\beta^2} + \frac{A_2}{2\beta}. \end{aligned} \tag{33}$$

The statistics of $g_{k,n}$, can be derived by substituting the synchronization error model in Eq.(19) and the parameters of A_1, A_2 into Eq.(33). For the mean of $g_{k,n}$ for SL case is

$$\mu_g^{SL}(SINR_k^p, O_{k,n}) = \frac{1.125O_{k,n}^5 - 4.5O_{k,n}^4 + 4.5O_{k,n}^3}{\epsilon^6 L^2 (SINR_k^p)^2} + \frac{2O_{k,n}^3 - 6O_{k,n}^2 + 6O_{k,n}}{\epsilon^3 L SINR_k^p}, \tag{34}$$

where $\epsilon = \frac{L_1}{L}$ is the preamble ratio.

Similarly, the mean of g for WL case can be derived as:

$$\mu_g^{WL}(SINR_k^p, O_{k,n}) = \frac{-1.125O_{k,n}^5}{\epsilon^6 L^2 (SINR_k^p)^2} + \frac{2O_{k,n}^3}{\epsilon^3 L SINR_k^p}. \tag{35}$$

2) SECOND MOMENT STATISTICS,**VARIANCE**, σ_Z^2

By applying the rule of expectation of Gamma distribution to the nth power, $E[Y^n] = \frac{\Gamma(\alpha+n)}{\Gamma(\alpha)\beta^n}$, the second moment of the derived RV Z can be computed as

$$\begin{aligned}\sigma_Z^2 &= Var[Z; A_1, A_2] \\ &= E[Z^2] - E[Z]^2 \\ &= E[(A_1 Y^2 + A_2 Y)^2] - \mu_Z^2 \\ &= A_1^2 E[Y^4] + A_2^2 E[Y^2] + 2A_1A_2 E[Y^3] - \mu_Z^2 \\ &= A_1^2 \frac{\Gamma(\alpha+4)}{\Gamma(\alpha)\beta^4} + A_2^2 \frac{\Gamma(\alpha+2)}{\Gamma(\alpha)\beta^2} + 2A_1A_2 \frac{\Gamma(\alpha+3)}{\Gamma(\alpha)\beta^3} - \mu_Z^2. \end{aligned} \tag{36}$$

By substituting Eq.(33) and $\Gamma(n) = (n-1)!$ into Eq.(36), the second moment of Z then becomes

$$\sigma_Z^2(A_1, A_2) = \frac{6A_1^2}{\beta^4} + \frac{3A_1A_2}{\beta^3} + \frac{A_2^2}{2\beta^2}. \tag{37}$$

Therefore, by substitution the corresponding parameters into Eq.(37), the variance of the error model, $g_{k,n}$, is

$$\sigma_{g^{SL}}^2(\bar{A}_1^{SL}, \bar{A}_2^{SL}), \quad \sigma_{g^{WL}}^2(\bar{A}_1^{WL}, \bar{A}_2^{WL}). \tag{38}$$

As we can see in Eqs. (33) and (36), the first and second moments of the proposed residual error models are determined by parameters $A_1(O_{k,n}), A_2(O_{k,n})$ and $\beta(SINR_k^p)$, which are functions of overlapping degree, $O_{k,n}$, of the nth and kth packets, and the SINR of the strong (kth) packet preamble.

D. SINR EVALUATION OF MULTIPLE PACKETS OVERLAPPING

In this subsection, we describe how our method can be used iteratively to determine the SINR for each packet in a network level simulation. Each packet's SINR can be compared with a threshold to determine if the packet is decoded correctly. The threshold depends on the modulation type. The start times for packets (SOPs) and power levels for packets are typically computed in a Monte Carlo type network simulation, e.g., SOPs might be modeled using a Poisson process or some MAC protocol and power levels might be modeled using free space path loss for a given topology. Regardless of how the SOPs and powers are generated in the simulation, once they are known, instances of overlapping packets can be identified and for each instance, the overlapped packets can be sorted according to their powers. The procedure below can be used to evaluate $SINR_n$ in an instance of overlapped packets.

Algorithm 2 Iterative Approach for a Network-Level Type Simulation

1) Initialize the packet detection order counter, $k = 1$;
2) Compute the SINR the kth packet payload according to Eq.(5), using the previously generated $g_{i,j}$, that is, for $i = 1, \ldots, k-1$. Interferences from weaker uncanceled packets should be included.
3) Determine if the kth packet is decoded by comparing the payload SINR to the appropriate threshold. If not decoded, STOP. If decoded, proceed to next step.
4) Compute $SINR_k^P$, considering all the same interferences as in Step 2, but only consider the interferences that overlap to a significant extent with the preamble of Packet k.
5) Using a random number generator, generate the residual error factor to all the weaker packets, where $n = k+1, \ldots, n$, according to the statistical model in Eqs (26)-(31). When there is no interference on the preamble, $SINR_k^p = SNR_k$.
6) Increase the order counter, $n = n+1$, and go to Step 2) if $n < N$.

IV. SIMULATION RESULTS

A network-level simulation is considered out of the scope of this physical-layer centric paper; using the model in this paper, the authors are preparing another paper that reports a network-level simulation of a transmit-only wireless sensor network. In this section, the proposed metric REF g with/without (w/wo) approximation are simulated for the two-packet overlapping scenario (i.e., $N = 2$) with one-time IC. Therefore, we can drop the k, n subscript, where $SINR^p$ indicates the SINR of the strong packet preamble, while O indicates the overlapping between the two packets.

We evaluate the performance under three SNR values: 10dB, 15dB, and 20dB. The sample mean and variance of g without approximation, represented by Eqs.(10) and (12), are simulated and compared to the approximated mean as

in Eqs. (34) and (35) and variance as in Eq. (38) using 100,000 Monte Carlo trails.

A. STATISTICS OF g WITH RESPECT TO O

For the simulation results in Figs. 4, all solid curves are results for the mean based on the theoretical analysis in Section III-B without approximation, while all symbols represent corresponding statistics simulation based on the approximation analysis in Section III-C. As we can see, the mean of proposed practical residual error model matches the approximated analysis very well, with only few disagreements at the low overlapping degree O for low SNR because of the approximation of the phase error and the Taylor expansion error.

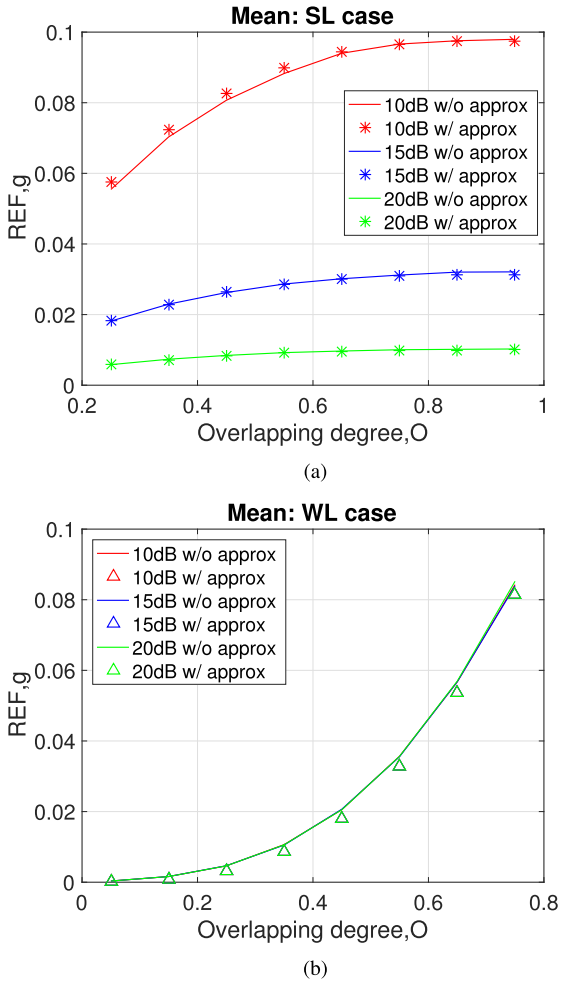

FIGURE 4. g versus overlapping degree, O with fixed $SINR = 7dB$. (a) Mean: SL case. (b) Mean: WL case.

According to the simulation results in Fig.4, the practical g for SL case increases with the growth of the overlapping degree, O but with decreasing slope, meanwhile affected by SNR of the strong packet. This is because, there is no interference on preamble for the SL case when $O > \epsilon = 0.25$. In other words, the SINR on the preamble equals the SNR of the packet, that is, $SINR^p = SNR$. As $g = ESR * O$, the slope indicates the ESR, which determined by the averaged residual error power over the interference interval. We observe that the red (top) curve in Fig.4a is approximately a scaled version of blue (middle) curve. We observe that the red (top) curve in Fig.4a is approximately a scaled version of blue (middle) curve. We think the slopes are more exaggerated in the red curves because the errors are generally larger for low SNR. The highest slope occurs at small overlaps for SL because the highest instantaneous residual error is always captured first. The slope decreases with the overlapping degree, O, with similar trend as ESR.

B. STATISTICS OF g WITH RESPECT TO SINR

On the other hand, the statistics of the WL case with interference on the preamble increases with the growth of the overlapping degree O but with a increased slope, and stays constant at different SNR. This happens because the SINR of the strong packet preamble matters than the SNR for the WL case. And the lowest instantaneous residual error is always captured first, which makes the slope or the ESR decrease over O.

The variances curves have the similar shape as the corresponding mean curves.

In Fig.5, with fixed overlapping degree, O, the statistics of the SL case are constant with respect to $SINR$ but decrease with growth of SNR, as we expected. This is because of the synchronization performance improves with the increase of the preamble SINR, which is just SNR when there is no interference. We also observe the small disagreements of the mean for SL case between without approximation and with approximations, indicated by the red curve and dots. This is caused by the approximation of the phase error and the Taylor expansion error at relative low SNR. On the other hand, the statistics of g for WL case decrease with the growth of SINR, but are same at different SNR, as expected.

C. THE DISTRIBUTION OF THE PRACTICAL RESIDUAL ERROR FACTOR, g

In this subsection, we simulate the distribution of the practical residual error factor g. The sample distribution based on the synchronization error model represented by Eq.(19) is compared with the theoretical analysis result in Eq.(31) at fixed SNR, SINR, and overlapping degree. According to the simulation results in Fig.6, the distribution of practical residual error matches our theoretical analysis.

V. EXPERIMENT DESIGN AND MEASUREMENTS

In this section, we design and conduct a large number of experimental trials to measure the defined metric ESR, based on the successful decoding sets with BER of zero. We employ three software defined radios (SDRs), as shown in Fig.7, to conduct the experiment. Two of them are the transmitters, and the other one is a GW. The are connected through cable, power splitter, and attenuators to create a controlled stationary channel.

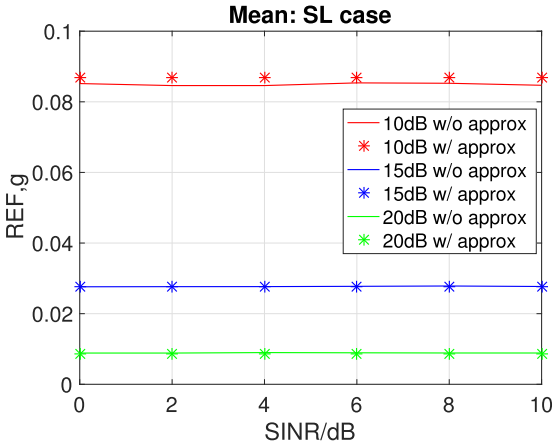

(a)

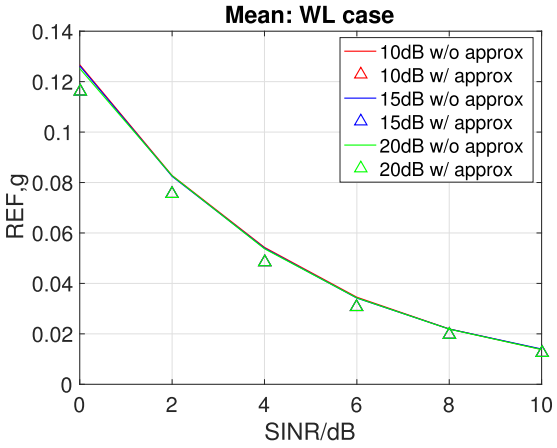

(b)

FIGURE 5. **g versus *SINR* with fixed overlapping degree, *O* = 0.5. (a) Mean: SL case. (b) Mean: WL case.**

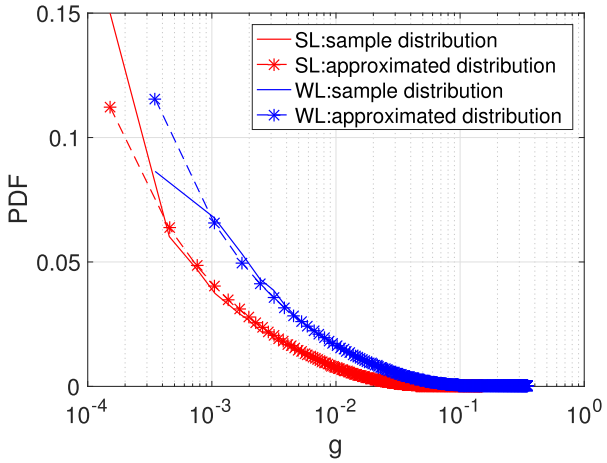

FIGURE 6. **Simulation on the distribution of of $g(SINR^p, O)$ at $SNR = 20$dB, $SINR = 7$dB, overlapping degree$O = 0.5$.**

A. EXPERIMENT DESIGN

1) PACKET SCHEDULING RULE

According to the theoretical analysis in Eq.(8), we know the practical residual error is determined by synchronization performance and channel estimation performance, as well as signal and noise powers. Therefore, we design the experiment

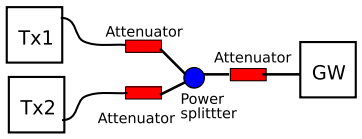

(a)

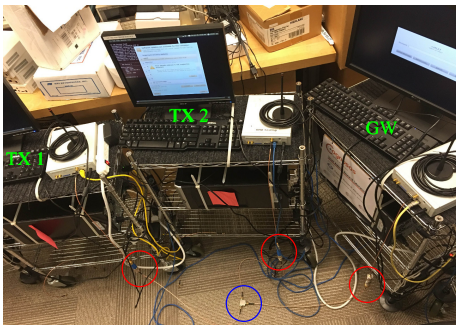

(b)

FIGURE 7. **Illustration of experiment setup. (* antenna was disabled for the experiments; red circle: attenuator; blue circle: power splitter.). (a) The diagram of experiment setup. (b) The photo of experiment setup.**

in terms of a set of packets, as illustrated in Fig.8, to evaluate the residual error in terms of SNR, SINR, and random overlapping scenario. As shown in Fig.8(a), the two TXs are scheduled to transmit packets continuously at different repetition rates once activated at time $t_{0,1}$ and $t_{0,2}$, respectively. By controlling the delay between the start times $t_\Delta = |t_{0,1} - t_{0,2}|$, we are able to create different overlapping degree situations. When TX1 with repetition rate $R_1 = \frac{1}{3}$ transmits at lower power, and TX2 with repetition rate $R_2 = \frac{1}{5}$ transmits at higher power, this results in the pattern or set in Fig.8(b); this pattern repeats. Each set contains both overlapping cases SL and WL, for a particular overlapping degree, O. We also have one interference-free reference of the strong packet and three interference-free references of the weak packet for each set.

In the experiment, we do not have access to instananeous residual error $e_s[i]$. Instead, we measure random outcomes of ESR, approximated as

$$ESR = \frac{|E\{|\hat{y}_w|^2\} - E\{|y_w|^2\}|}{E\{|\hat{y}_s|^2|\} - \hat{\sigma}_n^2}, \tag{39}$$

where $\hat{y}_w$ is a weak packet with residual error after subtracting of strong packet, y_w is an interference-free weak packet, $\hat{y}_s$ is the overlapping part of an interference-free strong packet, and $\hat{\sigma}_n^2$ is the estimated noise power.

TABLE 1.

Carrier frequency	430MHz
Sampling rate	$F_s = 200KHz$
Samples per symbol	$N = 32$
Modulation	MSK
Preamble ratio	$\epsilon = 0.25$

The symbols used in this paper are listed in Table 1. Each packet has the same payload of 48 MSK symbols and the

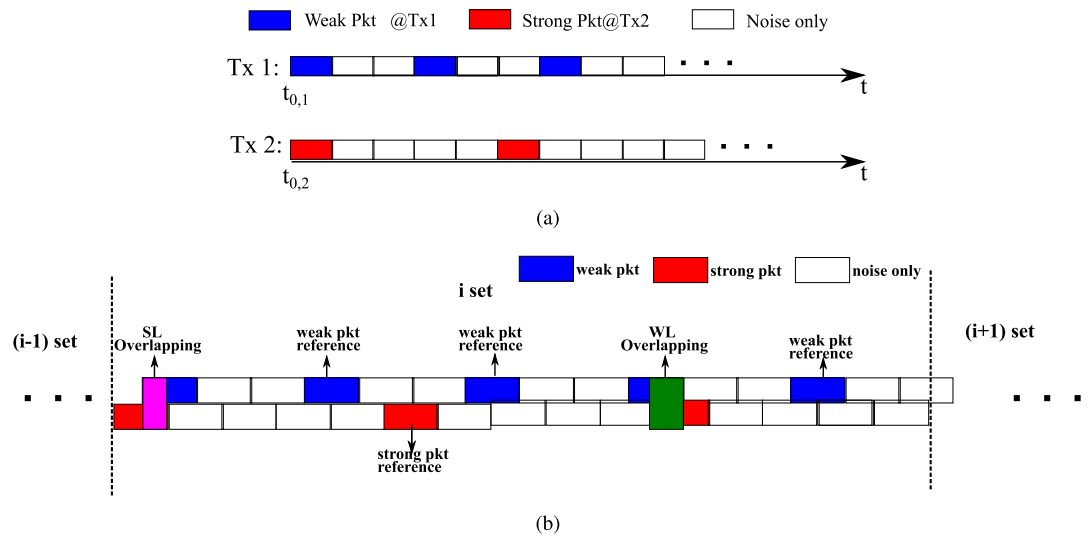

FIGURE 8. Illustration of experiment design. (a) Packet transmission schedule. (b) Designed received signal at GW.

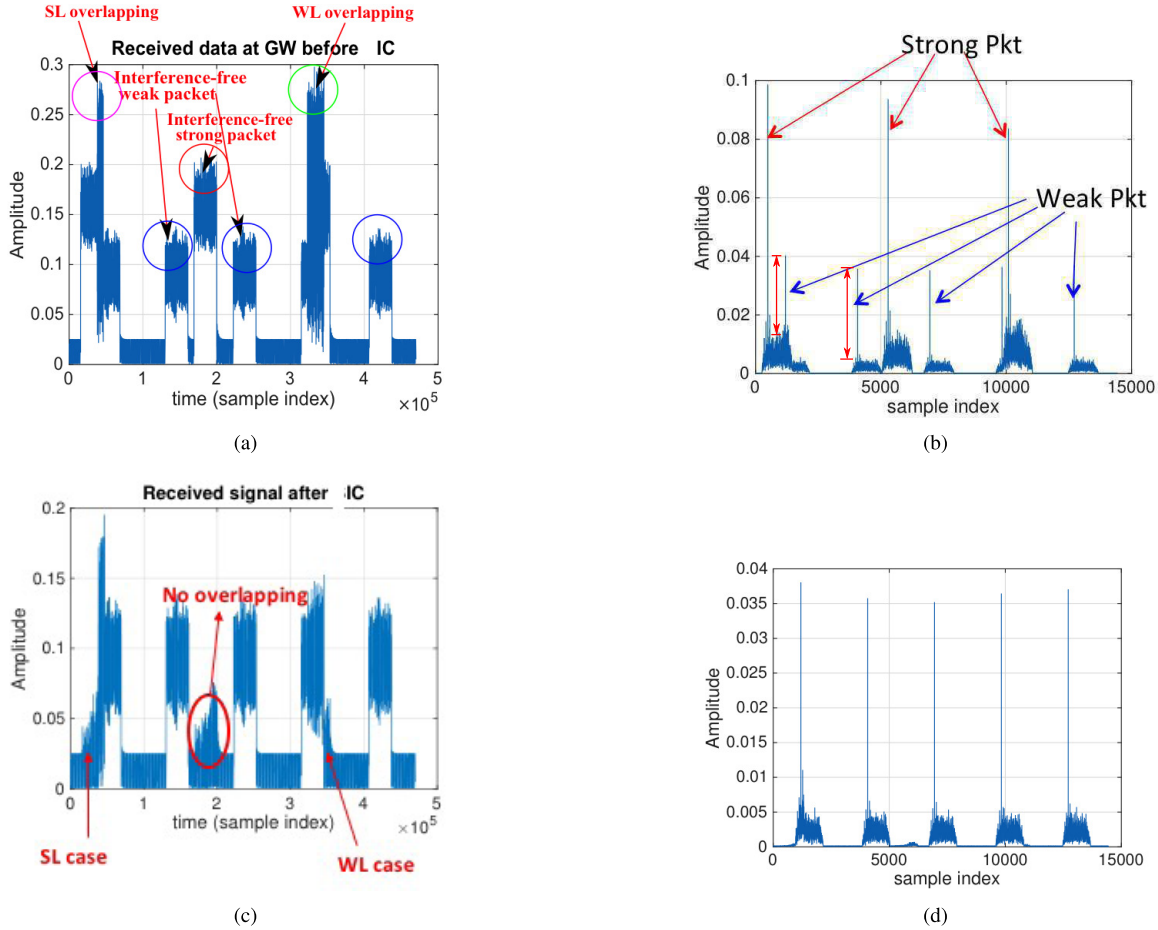

FIGURE 9. The received signal at GW for IC processing. (a) Amplitude of received signal before IC. (b) Amplitude of SOP metric before IC. (c) Amplitude of received signal after IC. (d) Amplitude of SOP metric after IC.

same preamble of 16 MSK symbols. Other system parameters for the experiments are listed in the table below. Different groups of sets have different transmitter power levels and overlapping degrees. We calculate the average residual error factor ESR based only on the successfully decoded sets with BER of zero. Each average is based on 200 sets.

2) EXPERIMENTAL INSTANTANEOUS RESIDUAL ERROR

Fig.9(a) shows the experimentally received signals, which match the set definition in Fig.8(b). The corresponding packet detection metric is shown in Fig.9(b) with the peaks indicating the starts of packets (SOPs). The peaks for the strong packets are higher than for the weak packets. The red double-ended arrows in Fig.9(b) indicate the difference between the peak of the metric and the "noise" level near the peak; this difference is proportional to the SINR of the preamble. Thus Fig.9(b) reflects that the preamble for the second weak packet, which is an interference-free reference, has a higher SINR than the preamble of the first weak packet, which has interference.

According to the measurements after IC processing in Figs.9(c) and 9(d), we find the instantaneous residual error is not constant over the packet but tends to initially worsen over time in Fig.9(c) as we expected based on Eq.(8). The error is small at the beginning because the channel estimate based on the preamble compensates for the initial phase offset. As we can see in Fig.9(d), we only see clear peaks indicating the SOPs of weak packets, which demonstrates the effectiveness of the cancellation and ability of the preamble correlation inherent in SOP estimation to suppress the interference from the residual error. Meanwhile, the weak packets are decoded without error after IC.

B. EXPERIMENT ESR

In this section, we conduct experiments to demonstrate the effects of SNR and SINR by controlling the TX powers of the overlapping packets. The scatter plots in Fig.10 a and b show ESR computed for each of 200 sets vs. O, for SL and WL, respectively, for strong packet SNR = 18.96dB and SINR= 6.5dB. These scatter plots are qualitatively similar to scatter plots for other settings.

Fig.11 shows plots of the average ESR (left axis) and the average strong packet preamble SINR ($SINR^P$, right axis), each averaged over 200 sets, as a function of the overlap degree, O. The Fig. 10 cases include SL (solid curves with star symbols) and WL (dashed curves with circle symbols), for various TX power combinations that are distinguished by color and further described below. The SNRs are the nearly horizontal dashed lines and the SINRs are the nearly horizontal solid lines; these are displayed to show experimental repeatability for different values of O.

1) HIGH TX POWER

we first conduct the experiments at high power levels with $P^s = 0\ dBm$ and $P^w = -7dBm$. The corresponding residual error measurements are red curves shown in Fig.11 with measured SNR and SINR of the strong packet to be $18.96dB, 6.50dB$, respectively. We observe that when the overlapping degree grows, the corresponding averaged ESR decreases for the SL case, while it increases for the WL case. Intuitively, this happens because the instantaneous error is increasing but the ESR is averaged only over the

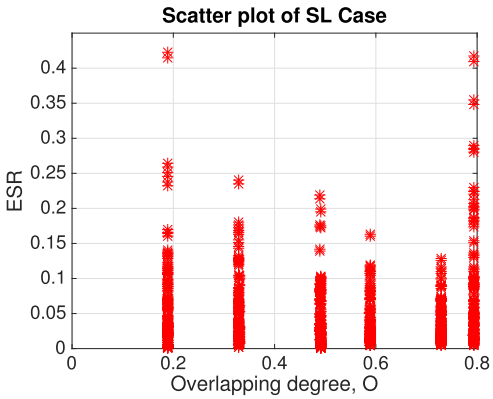

(a)

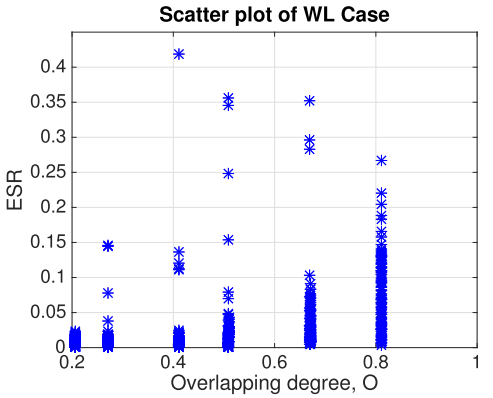

(b)

FIGURE 10. Scatter plot of measured ESR with $SNR = 18.96dB$, $SINR = 6.50dB$. (a) SL case. (b) WL case.

overlapping period. Thus, in the SL case, for small O, only the highest instantaneous error is captured in the average. On the other hand, in the WL case, for small O, only the lowest instantaneous errors are captured in the average. As O grows for the SL (WL) case, smaller (larger) values of the instantaneous error are averaged in, causing the downward (upward) trends in the graph. These results are consistent with Fig.4, recalling Eq.(10). We also observe that SL ESR goes up dramatically when $O = 0.8$. This happens because the preamble accounts for a quarter of the total packet. So when $O > 0.75$, the preamble of the strong packet for the SL case is also interfered so that synchronization and channel estimation performance are sacrificed.

2) LOW TX POWER

to demonstrate the effect of the SNR while keeping SINR approximately the same, we conduct experiments at the lower TX power levels of $P^s = -7dBm$ and $P^w = -14dBm$. The corresponding residual error measurements are blue curves shown in Fig.11 with measured SNR and SINR of the strong packet to be $11.98dB, 5.65dB$, respectively. We observe that when the SNR of the strong packet reduces, the corresponding ESR increases for the SL case, while it does not change much for WL case. This happens because the synchronization and channel estimation performances are mainly affected by

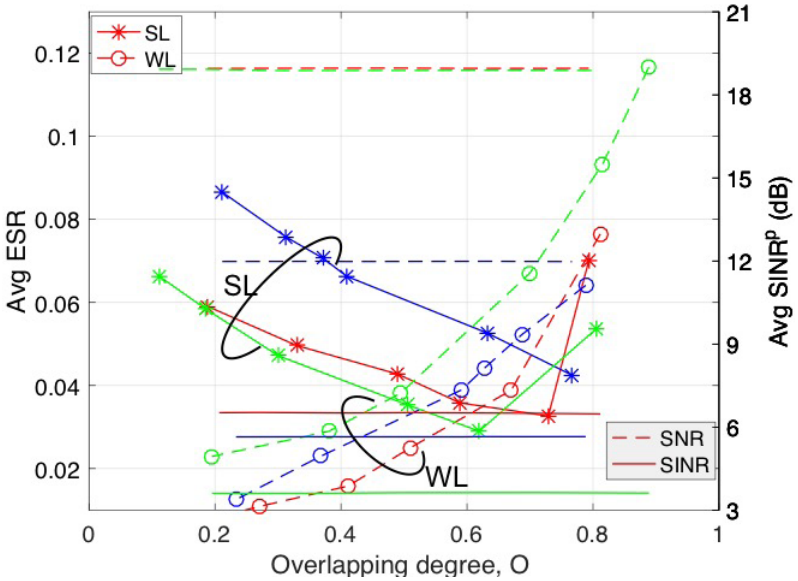

FIGURE 11. Measured average *ESR*.

the SNR for the SL case as there is no interference on the preamble, and the ESR grows as the synchronization performance gets worse with lower SNR. However for the WL case, the synchronization and channel estimation performances are mainly affected by the SINR.

3) SINR EFFECTS

to evaluate the SINR effects, we reduce the TX power difference from 7dBm to 4dBm. The TX powers are $P^s = 0dBm$ and $P^w = -4dBm$. The corresponding residual error measurements are green curves shown in Fig.11 with measured SNR and SINR of the strong packet to be $18.89dB$, $3.62dB$, respectively. By comparing the green curves and red curves, we observe that the ESR is similar to the SL case with star symbols, while it is worse for the WL case with circle symbols. This happens because when the SNR does not change much, the synchronization and channel estimation performances are similar for SL without interference on the preamble, but sacrificed for the WL case with interference on the preamble as SINR decreases.

VI. CONCLUSION

The residual interference or error after interference cancellation (IC), for overlapping constant envelope modulation, considering realistic synchronization, has been studied both analytically and experimentally. The distribution, the mean, and the variance of the IC residual error factor are derived. These statistics were shown to depend strongly on the overlap degree and the SINR of the preamble of the packet being canceled, which contrasts with the popular constant model of residual error factor. Experimental results show the same trends as the analytical results.

The IC residual error statistics derived in this paper are conditioned on the degree of packet overlaps and received powers of packets, which cannot be controlled in random topologies and in random access networks. However, for network simulation, with a specified network setup, such as a transmission pattern and path loss model, the statistics of the proposed residual error model could be used to evaluate the system level performance. We are preparing a future publication that uses the IC interference model to evaluate a transmit-only wireless sensor network. Ideas for future research include deriving unconditional statistics for random access networks which may, in turn, be used to derive network performance theoretically. In addition, the proposed residual error model could also be explored to guide the system design, such as, packet structure (e.g., duration and placement of preamble), in order to maximize the network throughput.

REFERENCES

[1] M. Varanasi and B. Aazhang, "Multistage detection in asynchronous code-division multiple-access communications," *IEEE Trans. Commun.*, vol. 38, no. 4, pp. 509–519, Apr. 1990.
[2] A. Duel-Hallen, "Decorrelating decision-feedback multiuser detector for synchronous code-division multiple-access channel," *IEEE Trans. Commun.*, vol. 41, no. 2, pp. 285–290, Feb. 1993.
[3] P. Patel and J. Holtzman, "Analysis of a simple successive interference cancellation scheme in a DS/CDMA system," *IEEE J. Sel. Areas Commun.*, vol. 12, no. 5, pp. 796–807, Jun. 1994.
[4] C. Stefanović, P. Popovski, and D. Vukobratovic, "Frameless ALOHA protocol for wireless networks," *IEEE Commun. Lett.*, vol. 16, no. 12, pp. 2087–2090, Dec. 2012.
[5] O. del Río Herrero and R. De Gaudenzi, "Generalized analytical framework for the performance assessment of slotted random access protocols," *IEEE Trans. Wireless Commun.*, vol. 13, no. 2, pp. 809–821, Feb. 2014.
[6] A. Zanella, A. Biral, and M. Zorzi, "Asymptotic throughput analysis of massive M2M access," in *Proc. Inf. Theory Appl. Workshop (ITA)*, Feb. 2015, pp. 64–69.
[7] J. G. Andrews and T. H. Meng, "Optimum power control for successive interference cancellation with imperfect channel estimation," *IEEE Trans. Wireless Commun.*, vol. 2, no. 2, pp. 375–383, Mar. 2003.
[8] J. G. Andrews, "Interference cancellation for cellular systems: A contemporary overview," *IEEE Wireless Commun*, vol. 12, no. 2, pp. 19–29, Apr. 2005.

[9] H. Lieske, G. Kilian, M. Breiling, S. Rauh, J. Robert, and A. Heuberger, "Decoding performance in low-power wide area networks with packet collisions," *IEEE Trans. Wireless Commun.*, vol. 15, no. 12, pp. 8195–8208, Dec. 2016.
[10] M. A. Weitnauer *et al.*, "Reliability and longer range for low power transmitters with on demand network MIMO," in *Proc. IEEE Int. Conf. RFID (RFID) (IEEE RFID)*, Orlando, FL, USA, May 2016, pp. 1–10.
[11] Cognosos Inc. *Data to the Cloud*. Accessed: Jan. 2018. [Online]. Available: http://www.cognosos.com
[12] Q. Lin, J. Lee, and M. A. Weitnauer, "Practical residual error of interference cancellation for spread MSK with a pseudo-noise preamble," in *Proc. IEEE Global Commun. Conf. (GLOBECOM)*, Dec. 2016, pp. 1–6.
[13] Y. Yan *et al.*, "WizBee: Wise ZigBee coexistence via interference cancellation with single antenna," *IEEE Trans. Mobile Comput.*, vol. 14, no. 12, pp. 2590–2603, Dec. 2014.
[14] M. Grieger, P. Marsch, and G. Fettweis, "Uplink base station cooperation by iterative distributed interference subtraction," in *Proc. IEEE 20th Int. Symp. Pers., Indoor Mobile Radio Commun.*, Sep. 2009, pp. 1973–1977.
[15] D. Halperin, T. Anderson, and D. Wetherall, "Taking the sting out of carrier sense: Interference cancellation for wireless LANs," in *Proc. 14th ACM Int. Conf. Mobile Comput. Netw.*, 2008, pp. 339–350.
[16] L. Kong and X. Liu, "mZig: Enabling multi-packet reception in zigbee," in *Proc. 21st Annu. Int. Conf. Mobile Comput. Netw.*, 2015, pp. 552–565.
[17] A. Hasan and J. Andrews, "Cancellation error statistics in a power-controlled CDMA system using successive interference cancellation," in *Proc. IEEE 8th Int. Symp. Spread Spectr. Techn. Appl.*, Aug. 2004, pp. 419–423.
[18] K. Zidane *et al.*, "Effect of residual channel estimation errors in random access methods for satellite communications," in *Proc. IEEE 81st Veh. Technol. Conf. (VTC Spring)*, May 2015, pp. 1–5.
[19] X. Xiong, K. Zheng, R. Xu, W. Xiang, and P. Chatzimisios, "Low power wide area machine-to-machine networks: Key techniques and prototype," *IEEE Commun. Mag.*, vol. 53, no. 9, pp. 64–71, Sep. 2015.
[20] J. Gubbi, R. Buyya, S. Marusic, and M. Palaniswami, "Internet of Things (IoT): A vision, architectural elements, and future directions," *Future Generat. Comput. Syst.*, vol. 29, no. 7, pp. 1645–1660, 2013.
[21] *CC1101*. Accessed: Nov. 2018. [Online]. Available: http://www.ti.com/product/cc1101
[22] *ADF7023*. Accessed: Nov. 2018. [Online]. Available: https://www.analog.com/en/products/adf7023.html
[23] *nRF905*. Accessed: Nov. 2018. [Online]. Available: http://www.nordicsemi.com/eng/Products/Sub-1-GHz-RF/nRF905
[24] W. Gao, *Energy and Bandwidth-Efficient Wireless Transmission*. Cham, Switzerland: Springer, 2017.
[25] C. Huebner, R. Cardell-Oliver, S. Hanelt, T. Wagenknecht, and A. Monsalve, "Long-range wireless sensor networks with transmit-only nodes and software-defined receivers," *Wireless Commun. Mobile Comput.*, vol. 13, no. 17, pp. 1499–1510, 2013.
[26] T. R. Park and M. J. Lee, "Power saving algorithms for wireless sensor networks on IEEE 802.15.4," *IEEE Commun. Mag.*, vol. 46, no. 6, pp. 148–155, Jun. 2008.
[27] P. Parsch, A. Masrur, and W. Hardt, "Designing reliable home-automation networks based on unidirectional nodes," in *Proc. 9th IEEE Int. Symp. Ind. Embedded Syst. (SIES)*, Jun. 2014, pp. 88–95.
[28] B. Firner, "Transmit only for dense wireless networks," Ph.D. dissertation, Rutgers Univ.-Graduate School-New Brunswick, New Brunswick, NJ, USA, 2014.
[29] Q. Lin, S. Mohan, and M. A. Weitnauer, "Interference-insensitive synchronization scheme of MSK for transmit-only wireless sensor network," in *Proc. IEEE Int. Conf. Commun. Wireless Commun. Symp. (ICC)*, May 2016, pp. 1–6.
[30] J. G. Proakis, *Digital Communications*. New York, NY, USA: McGraw-Hill, 1995.
[31] E. Hosseini and E. Perrins, "Timing, carrier, and frame synchronization of burst-mode CPM," *IEEE Trans. Commun.*, vol. 61, no. 12, pp. 5125–5138, Dec. 2013.
[32] A. Zygmund, *Trigonometric Series*, vol. 1. Cambridge, U.K.: Cambridge Univ. Press, 2002.
[33] A. Barbieri and G. Colavolpe, "On the cramer-rao bound for carrier frequency estimation in the presence of phase noise," *IEEE Trans. Wireless Commun.*, vol. 6, no. 2, pp. 575–582, Feb. 2007.
[34] N. Noels, H. Steendam, M. Moeneclaey, and H. Bruneel, "Carrier phase and frequency estimation for pilot-symbol assisted transmission: Bounds and algorithms," *IEEE Trans. Signal Process.*, vol. 53, no. 12, pp. 4578–4587, Dec. 2005.
[35] F. B. Hildebrand, *Advanced Calculus for Applications*, vol. 63. Englewood Cliffs, NJ, USA: Prentice-Hall, 1962.

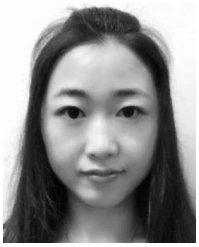

QIONGJIE LIN received the B.S. degree in communications engineering from the Nanjing University of Posts and Telecommunication, China, in 2012, and the M.S. and Ph.D. degrees in electrical and computer engineering from Georgia Tech in 2015 and 2017, respectively. From 2013 to 2017, she was a Graduate Research Assistant of Prof. M. A. Weitnauer at the SRAL. During her Ph.D. degree, she was working on physical layer system design and implementation of distributed arrays on software-defined radios for a variety of packet-based wireless systems, such as wireless LAN, *ad hoc*, and low-power wide area networks.

She is currently a Senior Standards Engineer at Samsung Research America Inc., Mountain View, CA, USA.

MARY ANN WEITNAUER (M'83–SM'03) joined the School of Electrical and Computer Engineering, Georgia Tech, as an Assistant Professor in 1989, where she is currently a Professor and a Senior Associate Chair. She was a Visiting Professor at Aalborg University, Aalborg, Denmark, from 2006 to 2008 and at Idaho National Labs in 2010. She held the Georgia Tech ADVANCE Professorship with the College of Engineering from 2006 to 2012. She has authored or co-authored over 200 refereed journal and conference papers. Her research is focused on the lower three layers of MIMO wireless networks that have virtual or distributed antenna arrays. Many results are demonstrated on a 20-node network of software-defined radios in practical environments and topologies. She received four best paper awards in conferences. She was an Associate Editor of the IEEE TRANSACTIONS ON MOBILE COMPUTING from 2009 to 2012.